An $Al_xIn_{1-x}As$/GaAs heterojunction ultra-thin film solar cell with 20% efficiency

K. A. S. M. Ehteshamul Haque*

Department of Electrical and Electronic Engineering, Islamic University of Technology Board Bazar, Gazipur1704, Bangladesh

(Received 13 October 2012)

An ultra-thin film photovoltaic cell, which incorporates an $Al_xIn_{1-x}As$/GaAs heterojunction, is simulated using Adept 1D simulation tool, and it is with an energy conversion efficiency of 20.06% (under 1 sun, AM1.5G illumination) for 604 nm cell thickness (excluding the substrate thickness), and optimized layer thickness and doping concentration for each layer of the device. The device has an n-type AlAs window layer (highly doped), an n-type $Al_xIn_{1-x}As$ emitter layer and a p-type GaAs base layer. Germanium (Ge) substrate is used for the structure. The device parameters are optimized separately for each layer. Based on these optimizations, the ultra-thin film solar cell design is proposed after careful consideration of lattice mismatch between two adjacent layers of the device.

Document code: A **Article ID:** 1673-1905(2013)03-0177-4

DOI 10.1007/s11801-013-2375-1

III-V compounds have been widely used for fabricating ultra-high efficiency photovoltaic cells, especially multi-junction solar cells. But these cells are very expensive, compared with the commonly used terrestrial solar cells. So the use of III-V solar cells is still limited to space applications[1]. Utilization of such solar cells for terrestrial applications requires to reduce the costs of materials processing and fabrication. Ultra-thin film solar cells with high efficiency, which are fabricated with III-V compounds, can be an approach for the realization of terrestrial III-V solar cells. This paper presents a 1D simulation of an $Al_xIn_{1-x}As$/GaAs heterojunction thin film solar cell. $Al_xIn_{1-x}As$ has recently gained attention as the absorber of single-junction and multi-junction solar cells[2].

The window layer material is AlAs, which has a high indirect bandgap of 2.16 eV. It has a zincblende structure with a lattice constant of 0.566 nm. The emitter layer is composed of $Al_xIn_{1-x}As$, where x is finally adjusted to 0.47. $Al_{0.47}In_{0.53}As$ has a zincblende structure with a lattice constant of 0.58686 nm and a direct bandgap of 1.46 eV. The lattice mismatch between AlAs and $Al_{0.47}In_{0.53}As$ is 3.55%, which marginally allows the growth of 2 nm-thick AlAs epitaxial layer on $Al_{0.47}In_{0.53}As$ without considerable amount of defects[3]. The base layer material of GaAs is a direct bandgap material with a bandgap of 1.424 eV and an absorption edge at 870 nm. The high lattice mismatch between GaAs and $Al_{0.47}In_{0.53}As$ is 3.72%. Germanium is a widely-used substrate for heterojunction and multi-junction solar cells. Fig.1 shows a schematic diagram of the device.

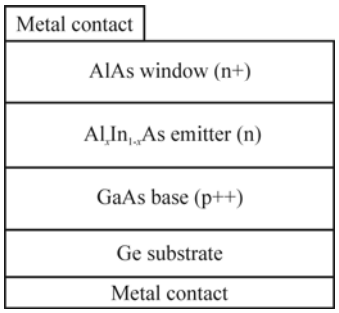

Fig.1 Schematic diagram of the $Al_xIn_{1-x}As$/GaAs heterojunction thin film solar cell

Adept[4] is a 1D simulation software which can simulate the electrical characteristics of heterostructured semiconductor devices. It is originally written to model solar cells fabricated from a wide variety of materials.

After choosing the materials for each layer of the device, some default values of device parameters (layer thickness and layer doping) are chosen arbitrarily. Tab.1 lists the default values. Simulation is conducted with these default values, and *J-V* characteristic curve is obtained for the solar cell. For all the simulations in this work, AM1.5G illumination (1000 W/m^2) at 1 sun is considered.

From the *J-V* curve, values of open-circuit voltage (V_{oc}) and short-circuit current density (J_{sc}) are obtained. Fill factor (*FF*) is calculated by[5]

$$FF = \frac{V_{ocn} - \ln(V_{ocn} + 0.72)}{V_{ocn} + 1}, \quad (1)$$

* E-mail: showmo082422@gmail.com

$$V_{ocn} = \left(\frac{q}{nkT}\right) V_{oc}, \quad (2)$$

where V_{oc} is the open-circuit voltage (in Volt), n is the ideality factor (taken as 1), k is the Boltzmann constant and T=300 K.

The efficiency (η) is given by

$$\eta = \frac{V_{oc} \times J_{sc} \times FF}{E} \times 100\%, \quad (3)$$

where E is the solar irradiance on earth in W/cm^2. Under AM1.5G, E= 0.1 W/cm^2.

Tab.1 Default values of device parameters

Device parameter	Window (AlAs)	Emitter ($Al_xIn_{1-x}As$)	Base (GaAs)
Layer thickness (μm)	0.01	100	5
Doping type	n	n	p
Doping conc.(cm^{-3})	1×10^{18}	1×10^{16}	1×10^{19}

Using Eq.(3), the energy conversion efficiency is calculated.

Aluminium mole fraction (x) in $Al_xIn_{1-x}As$ is varied between 0.2 and 0.6 in step of 0.1, and simulations are conducted for each of these alloy compositions. Tab.2 lists the simulation results. The efficiency versus alloy composition of $Al_xIn_{1-x}As$ is shown in Fig.2.

Tab.2 Outcomes for large scale variation of alloy composition in $Al_xIn_{1-x}As$

x in $Al_xIn_{1-x}As$	J_{sc} (mA/cm^2)	V_{oc} (V)	FF
0.2	49.83	0.3082	0.7261
0.3	42.35	0.5409	0.8140
0.4	33.18	0.7750	0.8571
0.5	24.52	1.0123	0.8832
0.6	17.84	1.2306	0.8996

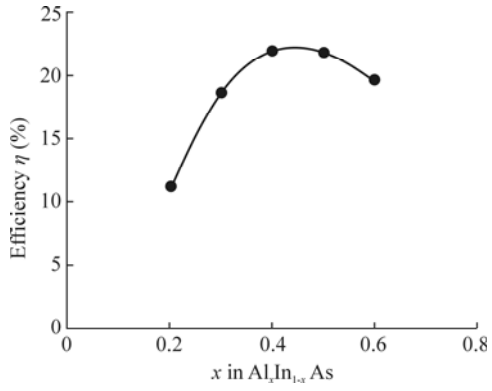

Fig.2 Efficiency vs. large scale variation of alloy composition in $Al_xIn_{1-x}As$

From Fig.2, it is evident that maximum efficiency is achieved when the aluminium mole fraction in $Al_xIn_{1-x}As$ is between 0.4 and 0.5. In order to find out the optimum value of x in $Al_xIn_{1-x}As$, further simulations are conducted by varying x from 0.45 to 0.49 in step of 0.01. The outcomes are given in Tab.3. Fig.3 shows the efficiency against the small scale variation of x in $Al_xIn_{1-x}As$ between 0.45 and 0.49. From the observation of Fig.3, x is adjusted at 0.47.

Tab.3 Outcomes for small scale variation of alloy composition in $Al_xIn_{1-x}As$

x in $Al_xIn_{1-x}As$	J_{sc} (mA/cm^2)	V_{oc} (V)	FF
0.45	28.90	0.8965	0.8719
0.46	28.46	0.9115	0.8735
0.47	27.72	0.9433	0.8768
0.48	26.78	0.9582	0.8782
0.49	25.68	0.9871	0.8809

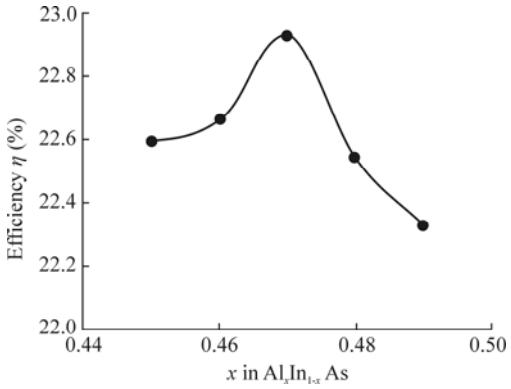

Fig.3 Efficiency vs. small scale variation of alloy composition in $Al_xIn_{1-x}As$

It has been observed that short-circuit current and optical properties of a solar cell are improved with a thinner window layer[6]. Moreover, the high lattice mismatch between AlAs and $Al_{0.47}In_{0.53}As$ (3.55%) demands that the epitaxial AlAs layer grown on $Al_{0.47}In_{0.53}As$ must be very thin. So a 10 nm-thick AlAs window layer is considered for further simulations. Now, a high doping level at the window layer reduces surface recombination of minority carriers coming from the emitter[7]. So high doping of 1×10^{18} cm^{-3} is maintained in the window layer.

Emitter layer thickness is varied within a wide range from 100 nm to 50 μm. Tab.4 shows the outcomes, while Fig.4 shows a graph of efficiency versus emitter layer thickness.

It is seen from Tab.4 that the open-circuit voltage increases with reduced emitter thickness. This occurs due to a reduction of saturation current with reduced cell geometry, and it was reported previously[8]. The short-circuit current initially increases with decreasing emitter thickness, but it goes down when emitter thickness is less than 2 μm. The highest efficiency of 27.28% is

achieved at a thickness of 1 μm, as shown in Fig.4. So the emitter thickness is adjusted to 1 μm.

Tab.4 Outcomes for varying emitter layer thickness

Emitter thickness (μm)	J_{sc} (mA/cm^2)	V_{oc} (V)	*FF*
50	29.08	0.9459	0.8770
20	30.32	0.9601	0.8784
10	30.61	0.9762	0.8799
5	30.69	0.9900	0.8812
2	30.70	1.0026	0.8824
1	30.64	1.0084	0.8829
0.5	30.51	1.0118	0.8832
0.4	30.46	1.0124	0.8832
0.1	30.17	1.0168	0.8836

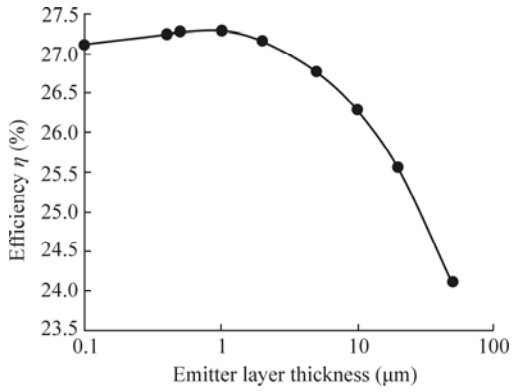

Fig.4 Efficiency vs. emitter layer thickness

Base layer thickness is varied between 1 μm and 50 μm. Tab.5 gives the outcomes, while a graph of efficiency versus base layer thickness is shown in Fig.5.

The thicker base can absorb a greater number of photons. So the efficiency is drastically reduced at lower base thickness. Now, a trade-off must be made between base thickness and efficiency. Fig.5 shows that the rate of efficiency increment drops when base thickness is larger than 5 μm. So a base thickness of 5 μm is considered for further simulations.

Doping concentration of the emitter layer is varied from 10^{16} cm^{-3} to 10^{19} cm^{-3}. Tab.6 lists the simulation outcomes. A plot of efficiency versus emitter doping level is given in Fig.6.

Tab.5 Results for varying base layer thickness

Base thickness (μm)	J_{sc} (mA/cm^2)	V_{oc} (V)	*FF*
50	30.84	1.0300	0.8848
20	30.83	1.0287	0.8847
10	30.78	1.0175	0.8837
5	30.64	1.0084	0.8829
1	29.43	0.9724	0.8796

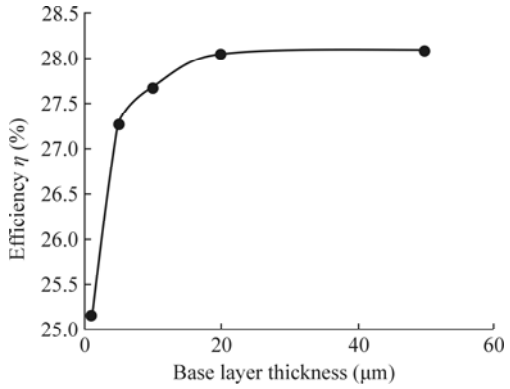

Fig.5 Efficiency vs. base layer thickness

Tab.6 Results for varying emitter doping level

Emitter doping conc. (cm^{-3})	J_{sc} (mA/cm^2)	V_{oc} (V)	*FF*
10^{16}	30.64	1.0084	0.8829
10^{17}	30.63	1.0176	0.8837
10^{18}	30.41	1.0188	0.8838
10^{19}	28.35	1.0225	0.8841

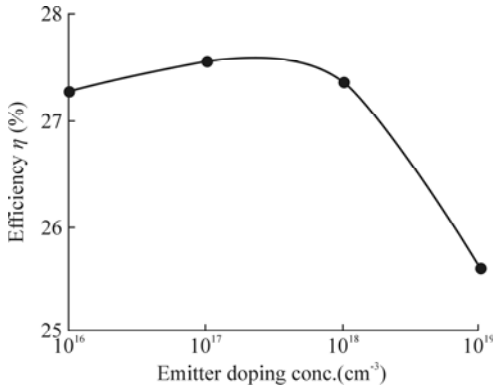

Fig.6 Efficiency vs. emitter doping level

Increasing the doping in the emitter enhances the electric field in the space-charge region of the n-p junction, which results in a higher open-circuit voltage. A higher electric field also increases the drift velocity of majority carriers, and increases the minority carrier recombination rate[9]. As can be seen from Fig.6, efficiency drops at very high emitter doping level (10^{18}–10^{19} cm^{-3}), which reveals that the increase of recombination rate dominates the increase of drift velocity at high doping levels. So for further simulations, a doping level of 10^{17} cm^{-3} is considered for the emitter.

Doping concentration at the base layer is varied between 10^{17} cm^{-3} and 10^{19} cm^{-3}. Tab.7 gives the simulation results, while Fig.7 shows the graph of efficiency versus base doping level.

As can be seen from Fig.7, efficiency is improved significantly at high base doping levels, which is a result of

simultaneous increment of V_{oc} and J_{sc} with increased base doping. So a very high doping level of 10^{19} cm^{-3} is kept at the base layer.

Tab.7 Outcomes for doping variation at the base layer

Base doping conc. (cm^{-3})	J_{sc} (mA/cm^2)	V_{oc} (V)	*FF*
10^{17}	28.77	0.7152	0.8483
10^{18}	30.42	0.8694	0.8689
10^{19}	30.63	1.0176	0.8837

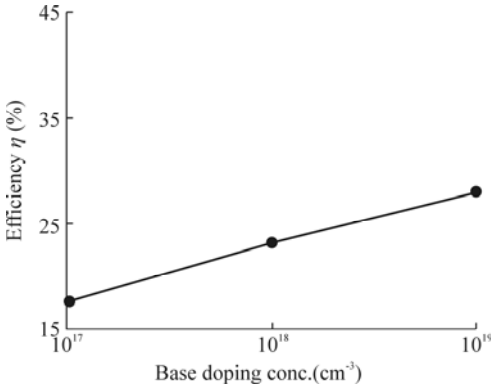

Fig.7 Efficiency vs. base doping level

AlAs has a lattice mismatch of 3.55% with $Al_{0.47}In_{0.53}As$, which limits the growth of AlAs on $Al_{0.47}In_{0.53}As$ by a critical layer thickness of 2 nm only[3]. As an ultra-thin window layer can provide the improved cell performance[6], a 2 nm window is acceptable for high efficiency. Lattice mismatch between $Al_{0.47}In_{0.53}As$ and GaAs is also considerably high (3.7%). This gives a critical layer thickness of around 2 nm for the growth of $Al_{0.47}In_{0.53}As$ on GaAs[3].

The GaAs base can be grown to be any desired thickness, as it is lattice-matched with Ge. But cost efficiency is a major issue. So the minimum cell thickness for achieving 20% efficiency is determined. Window and emitter layer thickness values are both kept as 2 nm, and simulations are conducted by varying the base thickness. Finally, an efficiency of 20.06% is achieved at a base thickness of 600 nm, which means a 604 nm-thick cell (excluding substrate thickness) achieves 20.06% efficiency. The resulting short circuit current density for this ultra-thin film solar cell is 23.7 mA/ cm^2, and the open-circuit voltage is 0.9632 V with a fill factor of 0.8786. The *J-V* characteristic curve for this case is shown in Fig.8.

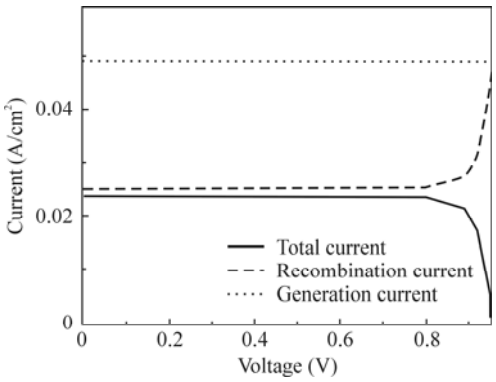

Fig.8 Light *J-V* characteristic curve for the ultra-thin film solar cell

This paper presents the introduction and detailed analysis of a thin film solar cell that utilizes a GaAs/ $Al_xIn_{1-x}As$ heterojunction as the working p-n junction of the cell. The efficiency obtained for the proposed solar cell is quite high, compared with the existing ultra-thin film solar cells. This design can be applied in the fabrication of single-junction solar cells, as well as for sub-cells in multi-junction solar cells.

References

[1] J. J. Schermer, G. J. Bauhuis, P. Mulder, E. J. Haverkamp, J. van Deelen, A. T. J. van Niftrik and P. K. Larsen, Thin Solid Films **511**, 645 (2006).

[2] M. S. Leite, R. L. Woo, W. D. Hong, D. C. Law and H. A. Atwater, InAlAs Epitaxial Growth for Wide Band Gap Solar Cells, IEEE Proc. 37th Photovolt. Specialists Conf., 780 (2011).

[3] R. People and J. C. Bean, Appl. Phys. Lett. **47**, 322 (1985).

[4] J. L. Gray and Michael McLennan, Adept, http://nanohub.org/resources/adept/, 2008.

[5] M. A. Green, Solid-State Electronics **24**, 788 (1981).

[6] M. S. Hossain, N. Amin, M. A. Matin, M. M. Aliyu, T. Razykov and K. Sopian, Chalcogenide Lett. **8**, 263 (2011).

[7] L. Aiguo, D. Jianning, Y. Ningyi, W. Shubo, C. Guanggui and L. Chao, J. Semicond. **33**, 023002 (2012).

[8] M. Wolf, High Efficiency Silicon Solar Cells, IEEE Proc. 14th Photovolt. Specialists Conf., 674 (1980).

[9] C. Lee, H. Efstathiadis, J. E. Raynolds and P. Haldar, Two-Dimensional Computer Modeling of Single Junction a-Si:H Solar Cells, IEEE Proc. 34th Photovolt. Specialists Conf., 1118 (2009).